THE JOURNAL OF BIOLOGICAL CHEMISTRY VOL. 290, NO. 10, pp. 6349–6360, March 6, 2015

Insulin-like Growth Factor 1 (IGF-1) Stabilizes Nascent Blood Vessels*

Received for publication, December 19, 2015 Published, JBC Papers in Press, January 7, 2015, DOI 10.1074/jbc.M114.634154

Sarah Melissa P. Jacobo and Andrius Kazlauskas[1]

From the Department of Ophthalmology, Harvard Medical School, The Schepens Eye Research Institute and Massachusetts Eye and Ear Infirmary, Boston, Massachusetts 02115

Background: Although both VEGF-A and IGF-1 promote angiogenesis, their relative contribution to neovessel stability is not completely understood.
Results: To generate stable tubes, VEGF-driven tube formation must be accompanied by IGF-1-mediated stabilization. The mechanism involves IGF-1-mediated prolonged activation of Erk, which antagonizes LPA-driven regression.
Conclusion: IGF-1 stabilizes VEGF-A-driven tube formation.
Significance: Anti-VEGF therapy can be complemented by approaches that modulate Erk or LPA pathways.

Here we report that VEGF-A and IGF-1 differ in their ability to stabilize newly formed blood vessels and endothelial cell tubes. Although VEGF-A failed to support an enduring vascular response, IGF-1 stabilized neovessels generated from primary endothelial cells derived from various vascular beds and mouse retinal explants. In these experimental systems, destabilization/regression was driven by lysophosphatidic acid (LPA). Because previous studies have established that Erk antagonizes LPA-mediated regression, we considered whether Erk was an essential component of IGF-dependent stabilization. Indeed, IGF-1 lost its ability to stabilize neovessels when the Erk pathway was inhibited pharmacologically. Furthermore, stabilization was associated with prolonged Erk activity. In the presence of IGF-1, Erk activity persisted longer than in the presence of VEGF or LPA alone. These studies reveal that VEGF and IGF-1 can have distinct inputs in the angiogenic process. In contrast to VEGF, IGF-1 stabilizes neovessels, which is dependent on Erk activity and associated with prolonged activation.

The formation of new blood vessels from the pre-existing vasculature (angiogenesis) is a deliberately orchestrated sequence of events that starts with destabilization of an existing vascular bed and ends when the newly generated vessels quiesce (1, 2). Much more is known about the formation of vessels compared with their stabilization and regression (3). Learning how to promote the regression of pathological vessels will potentiate current antiangiogenic approaches that target the formation of neovessels and, thereby, address the unmet needs of patients afflicted by diseases such as cancer or neovascular ocular disorders (4).

Extracellular cues that coordinate the angiogenic program include growth factors and bioactive lipids such as VEGF, PDGF, insulin-like growth factor 1 (IGF-1), and lysophosphatidic acid (LPA).[2] These angiomodulators make distinct contributions to angiogenesis. For instance, VEGF organizes endothelial cells into unstable vessels, whereas PDGF recruits pericytes that promote the maturation and stabilization of the neovessels (5).

So why are newly formed vessels unstable? The composition of angiomodulators in the microenvironment of the neovessels is a determining factor. For instance, angiopoietin 2 (Ang2) induces regression, provided that the level of VEGF is low (6–9). Similarly, LPA induces regression of nascent vessels (10–12). The fact that nascent vessels persist and mature suggests that the angiogenic process also involves steps to overcome the action of regression factors.

Studies in humans and mice indicate that IGF-1 plays an essential role in developmental angiogenesis (13–16). Although many cell types respond to IGF-1, endothelial cells are the key target in the context of developmental angiogenesis. Neovascularization is compromised when IGF-1R is deleted globally or specifically in the vascular endothelium (17, 18). The finding that IGF-1 enhances VEGF-dependent signaling events (13) begins to address the mechanism by which IGF-1 mediates its proangiogenic effects.

In contrast to the vast literature documenting the ability of IGF-1 to promote angiogenesis, there are few papers that consider if this phenomenon results from stimulating the formation of new vessels *versus* stabilizing them and, thereby, prevents their regression. The data presented in this work indicate that IGF-1 stabilizes endothelial cell tubes and retinal neovessels that form in response to VEGF. Furthermore, IGF-1 appears to accomplish this task by antagonizing signaling pathways that are engaged by the regression factor LPA. Our findings clarify at least one way in which IGF-1 promotes angiogenesis: by stabilizing neovessels.

EXPERIMENTAL PROCEDURES

Reagents—Lysophosphatidic acid (18:1) was purchased from Sigma-Aldrich (L-α-lysophosphatidic acid, oleoyl sodium salt, catalog no. L7260) and solubilized in methanol or chloroform:

* This work was supported by a Knights Templar Eye Foundation Early Career Award (to S. M. P. J.).
[1] To whom correspondence should be addressed: Tel.: 617-912-2517; Fax: 617-912-0101; E-mail: andrius_kazlauskas@meei.harvard.edu.
[2] The abbreviations used are: LPA, C18:1 lysophosphatidic acid; HMREC, human microvascular retinal endothelial cell; HCEC, human choroidal endothelial cell; P, postnatal day; DUSP, dual-specificity phosphatase; ANOVA, analysis of variance; ATX, autotaxin; ROCK, Rho-associated coiled-coil containing protein kinase.

methanol:acetic acid (95:5:5) to a stock concentration of 1 mg/ml. The stocks were aliquoted, dried in a Speedvac for storage at 4 °C, or used immediately. For cell-based assays, LPA was used at a final concentration of 10 μM by reconstituting the stock aliquot to 1 mM in sterile PBS supplemented with 0.1% fatty acid-free bovine serum albumin (Roche Diagnostics, catalog no. 10735078001). Recombinant human IGF-1 (Peprotech, catalog no. 100-11) was dissolved in 10 mM citric acid (pH 3.0) supplemented with 0.1% BSA and stored at −80 °C at stock concentrations of 100 ng/μl until use. Recombinant human VEGF-A 165 (R&D Systems, catalog no. 293-VE) was prepared according to the instructions of the manufacturer. The lyophilized solid was dissolved in PBS with 0.1% BSA to make a 100 ng/μl stock and then stored at 4 °C. The IGF-1 Receptor I tyrosine kinase inhibitor NVP-AEW541 (used at 1 μM) was from Cayman Chemicals (Ann Arbor, MI). The insulin-mimetic peptide antagonist to the insulin receptor, S961 (used at 100 nM), was from Phoenix Pharmaceuticals, Inc. (Burlingame, CA).

Cell Culture—Human microvascular retinal endothelial cells (HMRECs) were purchased from Cell Systems Corp. (Kirkland, WA) and used from postnatal day 6 (P6) to P10 for all experiments. Human umbilical vein endothelial cells were purchased from Clonetics (San Diego, CA) and used up to P8. Human choroidal endothelial cells (HCECs) were provided by Dr. Mary Elizabeth Hartnett (University of Utah) and used until P6. Bovine microvascular retinal endothelial cells were isolated from 3-month-old bovine eyes (Research 87, Inc., Boylston, MA) and used at P4-P10. Cells were plated on tissue culture dishes coated with 0.2% gelatin (Sigma) and maintained in M199 medium that contained 20% bovine calf serum (Hyclone, Logan, UT), 100 μg/ml heparin, 12 μg/ml bovine pituitary extract (Hammond Cell Tech, Windsor, CA), and 100 units/ml penicillin G and 100 μg/ml streptomycin C (Gemini Bioproducts, West Sacramento, CA) as described previously (19, 20). Cell culture medium was replaced every 2 days unless cultures needed to be passaged for *in vitro* tube assays.

Endothelial Tube Regression Assay—For endothelial tube length quantification and immunofluorescence staining, all assays were performed in 96-well plates. For regression studies, endothelial tubes were generated as described previously (19, 20) with a few modifications. 48 h prior to the tube regression assay, cells were collected in trypsin (0.5% in EDTA, 2 min at 37 °C). The suspension was neutralized with an equal volume of medium, centrifuged at 2000 rpm for 2 min, and then the pelleted cells were resuspended in M199 medium that contained 10% bovine calf serum (no heparin or bovine brain extract). Cells were dispensed in 100-μl aliquots on 70 μl of collagen gel at a density of 45×10^3 cells/well (10×10^3 for HCECs) and allowed to attach overnight. 16 h after plating, the culture medium was removed, the cells were washed carefully with PBS, and 30 μl of collagen gel mix was added and allowed to solidify for 1 h at 37 °C. The collagen gel consisted of 80% PureCol collagen (Advanced Biomatrix, Inc., San Diego, CA); 0.5 μg/ml of fibronectin (catalog no. F1141) and 0.5 μg/ml laminin (catalog no. L2020), both from Sigma-Aldrich; 20 mM HEPES; 2 mg/ml $NaHCO_3$; and 0.02 M NaOH. Endothelial tube formation was stimulated by overlaying the collagen sandwich with endothelial basal medium (Lonza, catalog no. CC-3121) supplemented with 5% horse serum and adding 2.5 ng/ml VEGF-A. Endothelial tubes that formed in this manner persisted overnight (16 h after the initial VEGF-A addition). No significant remodeling (changes in tube length or branch points) was observed from 8–16 h within VEGF-A stimulation, and tubes within this period were considered stable. On the day of the tube regression assay ("time 0" or 16 h after VEGF-A addition), the culture medium was removed, tubes were rinsed three times with PBS, and serum-free endothelial basal medium containing treatments for regression was added. In assays where antagonists were present, the pre-existing tubes were pretreated for 15 min with the antagonist alone before the regression assay treatments were added with the antagonists. The autotaxin inhibitor HA-130 and the pan-LPA receptor antagonist 1-bromo-3(*S*)-hydroxy-4-(palmitoyl)butyl-phosphonate (BrP)-LPA were from Echelon Biosciences (Salt Lake City, UT). The pan-LPA inhibitor Ki16425 was from Cayman Chemicals. The end point of regression assays was 4 h after addition of the treatments unless indicated otherwise. Data are represented as mean ± S.E. of at least three independent experiments, and each experiment was performed in quadruplicate wells.

Collection of Tube Lysates and Immunoblot Analysis—HMREC tubes were generated in a 24-well scale as described above. We prepared HMREC tube lysates as described previously (10, 12, 21). Briefly, medium was removed, and the collagen gel sandwich was digested with two gel volumes of collagenase (type I from *Clostridium histolyticum*, Sigma-Aldrich) in Hanks' buffered salt solution supplemented with 100 μM Na_3VO_4. The collagen gel was digested for 1 h at 37 °C or until the gels had dissolved visibly while the tubes still remained intact. For each time point, samples from five wells were pooled. The suspensions were collected in 2-ml microspin tubes and centrifuged at 500 × *g* for 2 min. The supernatant containing digested collagen was removed, and the pellet containing the tubes was washed twice with ice-cold PBS. The tubes were lysed on ice for 20 min with 90 μl of 2× lysis buffer (100 mM NaCl, 1% Triton X-100, 0.5% sodium deoxycholate, 0.2% SDS, 2 mM EDTA, 10 mM HEPES (pH 7.5), 1 mM Na_3VO_4, 10 mM NaF, 10 mM $Na_2P_2O_5$, and 1 mM PMSF) and clarified by centrifugation at 6000 × *g* for 2 min. Total protein concentrations were determined by BCA assay. The typical yield per sample (5 wells pooled together) was <2 mg/ml. A total of 20 μg of protein was loaded per lane on SDS-PAGE gel. For Western blot analysis of total cell lysates, pErk1/2 was probed with a rabbit monoclonal antibody against Thr-202/Tyr-204 (catalog no. 4370S, Cell Signaling Technology, Danvers, MA), pan-Erk1/2 was probed with a rabbit polyclonal antibody (catalog no. 9102, Cell Signaling Technology), and HRP-conjugated goat anti-rabbit IgG was from Santa Cruz Biotechnology (catalog no. sc-2004, Santa Cruz, CA). Films were scanned and saved in 8-bit grayscale at 300 pixels per inch resolution. Densitometry analysis was performed using the gel function of NIH ImageJ. Data are representative of $n = 3$ (for panels treated with VEGF-A) to 6 independent experiments.

Immunofluorescence Staining of Endothelial Tubes—HMRECs were subjected to tube regression assays as described above. For each independent experiment ($n = 3$), all treatments

were done in duplicate. At the indicated time points, treatments were removed, and the collagen gel was digested with two gel volumes of type I collagenase in Hanks' buffered salt solution with Na_3VO_4. The collagen gel was digested for 30 min at 37 °C or until the collagen gels had visibly reduced thickness while still preserving the structure of the endothelial tubes. Collagenase was removed carefully, and the intact tubes were washed 3 × 15 min with Na_3VO_4-supplemented ice-cold PBS. Tubes were fixed with 4% ice-cold paraformaldehyde for 10 min and washed with PBS 3 × 15 min. Tubes were blocked overnight at 4 °C with PBS containing 4% BSA, 10% goat serum (Sigma-Aldrich, catalog no. G9023), and 0.5% Triton X-100. pErk1/2 was probed with a rabbit monoclonal antibody (1:100 dilution, catalog no. 4370S, Cell Signaling Technology), and endothelial tubes were costained with Alexa Fluor 594-conjugated *Griffonia simplicifolia* isolectin B4 (1:100 dilution, catalog no. I21411, Invitrogen) overnight at 4 °C. For negative control, an equal molar dose of non-immune rabbit IgG (catalog no. sc-2027, Santa Cruz Biotechnology) was used in place of the pErk1/2 antibody. After primary antibody incubation, tubes were rinsed 3 × 15 min and incubated with Alexa Fluor 488-conjugated Affinipure goat anti-rabbit IgG (1:200 dilution, Jackson ImmunoResearch Laboratories, catalog no. 111-165-003) overnight at 4 °C. Tubes were rinsed 3 × 15 min. To prepare slides, the collagen gels were removed carefully from the 96-well plates by rimming the perimeter with straight Dumont #5 forceps (F.S.T. Instruments, Foster City, CA). The collagen gels were mounted on Ultra™ Frost glass slides (Denville Scientific, Inc., South Plainfield, NJ) with Vectashield mounting medium containing DAPI (Vector Laboratories, Inc., Burlingame, CA).

Laser-scanning Confocal Imaging—Images are representative of three independent experiments, and all conditions were done in duplicate wells. For each well, three to five randomly selected fields were imaged by sequential scanning of each channel using a Leica upright DM 6000S confocal laser-scanning microscope. Images at ×200 magnification were acquired from optical slices of ~10 μm using Leica Application Suite AF software v. 1.3.1. Confocal images for pErk1/2 are presented in monochrome for better contrast to facilitate qualitative intensity comparisons across different time points and treatments. IB4 and DAPI channels were merged using GIMP for Mac OS X.

HMREC Tube Total RNA Isolation and Real-time RT-PCR—Preformed HMREC tubes on a 24-well scale were washed three times with PBS and stimulated with the indicated treatments. After 30 min, the stimuli were removed by aspiration, the tubes were rinsed with ice-cold PBS, and total RNA was extracted using TRIzol reagent. For each treatment, six wells were pooled together to collect enough RNA. The typical yields were 250 ng/μl.

For real-time RT-PCR analysis of DUSP transcripts, the following PCR primers were obtained from the Massachusetts General Hospital PrimerBank and Oligo Synthesis Core Facility (Boston, MA): *DUSP1* (NM_004417), ACCACCACCGTGTTCAACTTC (forward) and TGGGAGAGGTCGTAATGGGG (reverse); *DUSP2* (NM_004418), TGCCCCAACCACTTTGAGG (forward) and AGTCAATGAAGCCTATGGCCT (reverse); *DUSP4* (NM_001394), GGCGGCTATGAGAGGTTTTCC (forward) and TGGTCGTGTAGTGGGGTCC (reverse); *DUSP5* (NM_004419), GCCAGCTTATGACCAGGGTG (forward) and GTCCGTCGGGAGACATTCAG (reverse); *DUSP6* (NM_001946), GAAATGGCGATCAGCAAGACG (forward) and CGACGACTCGTATAGCTCCTG (reverse); *DUSP7* (NM_001947), GACGTGCTCGGCAAGTATG (forward) and GGATCTGCTTGTAGGTGAACTC (reverse); *DUSP8* (NM_004420), TCAGCTCCGTCAACATCTGC (forward) and CGCGTGCTCTGGTCATAGA (reverse); and *GAPDH* (NM_002046), GGAGCGAGATCCCTCCAAAAT (forward) and GGCTGTTGTCATACTTCTCATGG (reverse). The design of the one-step PCR using Power RNA-to-Ct SYBR Green Mix (Applied Biosystems) with 100 ng of total RNA as template was first tested using a 40-cycle reaction in a benchtop thermocycler. The expected amplicons were validated by running PCR products on a 2% agarose gel. Quantitative real-time RT-PCR was performed on an Eppendorf Realplex 2. Relative expression of DUSP transcripts was calculated using the $2^{-\Delta\Delta CT}$ method relative to GAPDH and normalizing with vehicle control. Data represent mean ± S.E. of three experiments. Each experiment was performed in duplicate.

Animals—The 8-week-old male C57Bl/6J mice (Jackson Laboratories, Bar Harbor, ME) used in this study were acclimatized for at least 48 in the institute's animal facility in 12-h light-dark cycles with *ad libitum* access to food and water. The animals were euthanized by CO_2 narcosis. Animal handling procedures adhered to protocols approved by the Institutional Animal Care and Use Committee and the Association for Research in Vision and Ophthalmology Statement for the Use of Animals in Ophthalmic and Vision Research.

Murine Retinal Explants—We prepared retinal explants as described previously (10, 12, 22). Immediately after euthanasia, the eyes were enucleated and kept in PBS. The retinas were dissected under a Zeiss Stemi 2000-c stereomicroscope equipped with a KL 1500 LCD cold light source. When the retinas were dissected, four relaxing cuts were made to get four evenly sized quadrants. Each quadrant was further cut into four 1 × 1 mm pieces, yielding 16 pieces per eye for explants. Each piece was placed within a collagen gel (described above), with the ganglion cell layer facing up, in a 48-well tissue culture plate. The collagen gel sandwich was overlaid with endothelial basal medium containing 10% horse serum, 12 μg/ml bovine brain extract, 100 μg/ml heparin, and 25 ng/ml VEGF-A. Culture medium was replaced every 48 h after photographing the explants for phase-contrast image acquisition. Neovessel sprouting was typically observed starting on day 7, with significant and robust outgrowth starting on days 10–14. Thereafter, retinal explants with neovessel outgrowths that showed no significant or robust increase in length or caliber within a 48-h window were considered to be at their peak and stable (typically days 18–21). Retinal explants that reached this period were then treated with the indicated agents for regression assays.

For the experiments reported here (n = 3, 2 mice/experiment), the success rate of neovessel sprouting from retinal explants was 78–87%. Retinal explants of comparable robustness (number of neovessel outgrowths, length of sprouts) were selected for paired or grouped comparisons before adding the indicated treatments to minimize variability between explants from the same eye. In regression assays, culture medium that

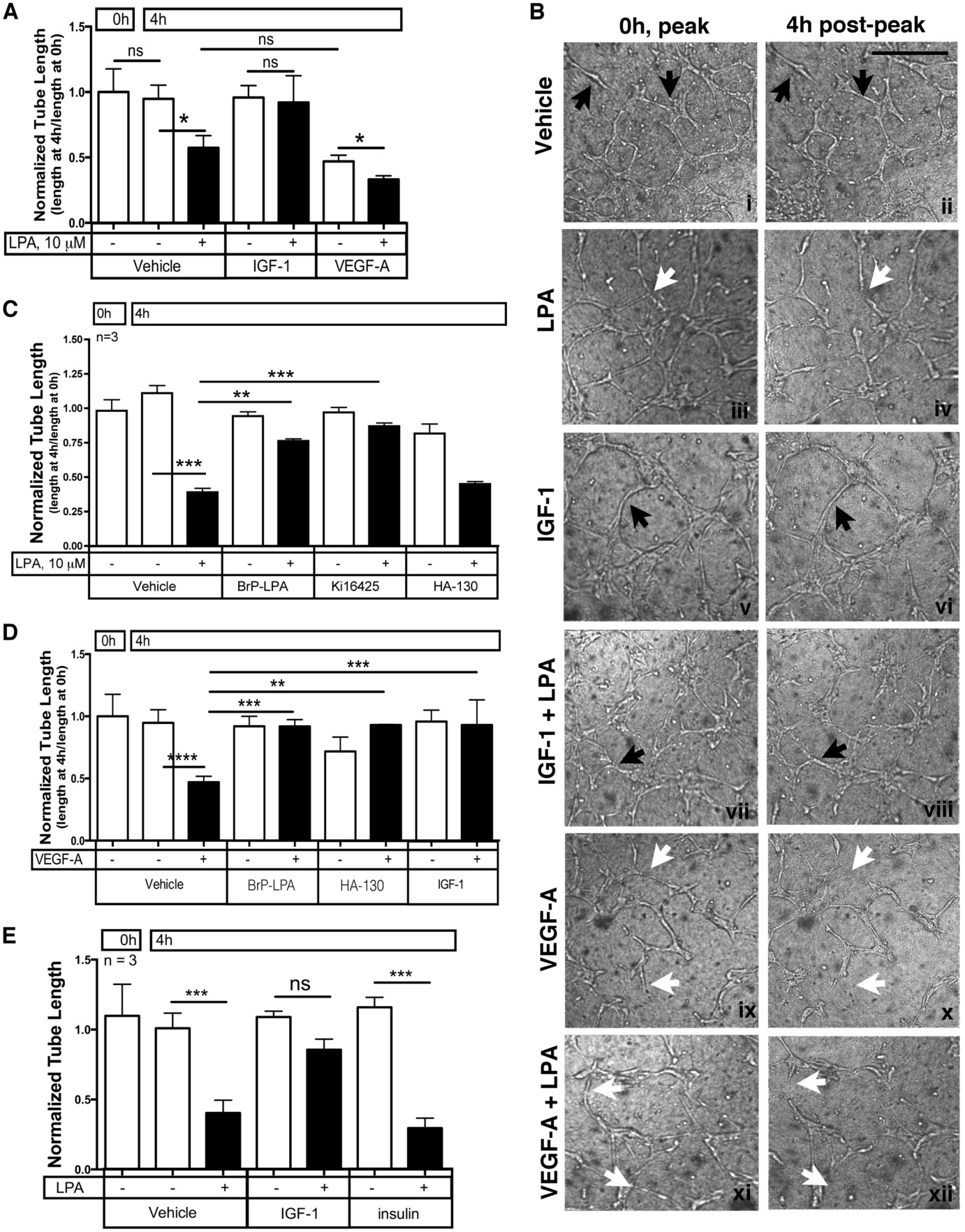
A
0h
4h
Normalized Tube Length
(length at 4h/length at 0h)
ns
ns
ns
*
*
LPA, 10 μM
Vehicle
IGF-1
VEGF-A
B
0h, peak
4h post-peak
Vehicle
LPA
IGF-1
IGF-1 + LPA
VEGF-A
VEGF-A + LPA
i
ii
iii
iv
v
vi
vii
viii
ix
x
xi
xii
C
n=3
***
**
***
Vehicle
BrP-LPA
Ki16425
HA-130
D
****
**
***
***
VEGF-A
Vehicle
BrP-LPA
HA-130
IGF-1
E
n = 3
***
ns
***
LPA
Vehicle
IGF-1
insulin

contained the indicated treatments were replaced every 12 h for 3 days. Data represent three independent experiments, and each experiment was done in duplicate. The explants were derived from the left and right mouse eye.

Image Analysis and Quantification—For tube assays and retinal explants, image acquisition and data quantification were performed as described previously (10, 12). Briefly, phase-contrast images at ×100 magnification were acquired with a Nikon Eclipse TE2000-S inverted microscope (Melville, NY) equipped with Diagnostic Instruments RT Slider charge-coupled device camera. 8-bit grayscale images at 1600 × 1400 ppi resolution were acquired using Spot Advanced for Mac OS X (Diagnostic Instruments, Sterling Heights, MI). Images were imported into National Institutes of Health ImageJ. For quantification of tube assays in a 96-well plate, a collected image was quantified by tracing the tubes using the brush tool (5-pixel brush width). The final values shown, "normalized neovessel length," represent the total pixel units at the end point (4 h) divided by the pixel units at the start (0 h, which is the peak of tube formation) of the regression assay. Each treatment was done in quadruplicate wells per independent experiment ($n = 3$ or more). For the visual representation of tubes in Fig. 1*B*, images were digitally zoomed ×8, and 1400 × 1400 ppi areas were selected randomly.

In retinal explant assays, phase contrast images at day 0 (start) and day 3 (end point) of regression assays were imported into National Institutes of Health ImageJ. Neovessels were traced using the paintbrush function, and total neovessel length was expressed as arbitrary pixel units. Normalized neovessel length represents the total pixel units at the end point (day 3) divided by the pixel units at the start (day 0, which is the peak of neovessel formation) of the regression assay. All representative images from each assay were prepared for figures using GIMP 2.8 for Mac OS X.

Data Analysis—Data analyses and graphing were performed with Prism 6.0 (GraphPad Software, San Diego, CA). Two-tailed Student's *t* test was used for paired comparisons. One-way analysis of variance followed by Tukey's post-hoc test was used for comparison of more than two groups. Comparisons in which $p < 0.05$ (*) at $\alpha \geq 0.05$ were considered statistically significant. ** denotes $p < 0.01$, and *** denotes $p < 0.001$.

RESULTS

VEGF-A Promoted Regression of Endothelial Tubes, whereas IGF-1 Stabilized Them—To study remodeling and destabilization of nascent capillaries *in vitro*, tubes were generated uniformly from primary HMRECs treated with VEGF-A in a modified version of the collagen gel sandwich assay described previously (19, 20). When such retinal endothelial tubes formed, they were stable and did not significantly remodel in terms of total length or branch points for at least 4 h in serum- and growth factor-free medium (Fig. 1, *A* and *B*) (12, 19). Adding purified LPA to such tubes induced regression (Fig. 1, *A* and *B*). As expected, LPA receptor antagonists (BrP-LPA or Ki16425) prevented regression, whereas an ATX inhibitor (HA-130) had no effect on this response because it was driven by exogenous LPA (Fig. 1*C*). Regression in this model system is not initiated by apoptosis, which is what happens to nascent tumor vessels when VEGF-A is acutely neutralized (24–26). Rather, LPA triggers regression by stimulating the migration and subsequent disorganization of tubes organized from primary endothelial cells (10–12).

In light of the existing observations that VEGF increases the level of ATX (10, 27, 28), we anticipated that VEGF would induce regression and that this response would be driven by LPA. Indeed, VEGF triggered regression of newly formed tubes (Fig. 1, *A*, *B*, and *D*). This response was blocked by antagonists of either LPA receptors or ATX (Fig. 1*D*), indicating that VEGF was acting via endogenously produced LPA.

In contrast to VEGF, IGF-1 failed to promote regression (Fig. 1, *A*, *B*, and *D*). This observation is consistent with the fact that IGF-1R does not engage PLCγ, which is activated by VEGFR2 and is required to increase the level of ATX (29, 30). Furthermore, IGF-1 prevented both VEGF- and LPA-stimulated regression (Fig. 1, *A*, *B*, and *D*). In contrast to IGF-1, insulin was unable to limit LPA-driven regression (Fig. 1*E*). Moreover, an IGF-1R-specific tyrosine kinase inhibitor (NVP-AEW541), but not an insulin receptor-specific antagonist (S961), abolished the IGF-1-mediated block of regression in the presence of LPA (data not shown).

The data in Fig. 1 reveal that VEGF promotes the regression of newly formed tubes and that the underlying mechanism is likely to involve the ATX-mediated production of LPA. Furthermore, IGF-1 not only failed to promote regression but antagonized this response.

IGF-1 Stabilized Tubes Organized from Four Types of Primary Endothelial Cells—In Fig. 1, regression was monitored in serum-free medium, and, under these conditions, this response was dependent on addition of LPA or agents that stimulated LPA production (such as VEGF-A). We sought to extend these findings to additional experimental conditions and types of endothelial cells.

In the presence of serum, tubes regress without addition of purified LPA because serum contains LPA, ATX, and the ATX

FIGURE 1. **IGF-1 prevented regression of endothelial tubes.** *A*, IGF-1 prevented LPA-stimulated regression of tubes. Endothelial tubes were generated by plating primary HMRECs between two layers of collagen and overlaying the collagen sandwich with serum- and VEGF-containing medium (see "Experimental Procedures"). Tubes formed and stabilized within 16 h under these conditions. The tubes were photographed (0 h, "peak"), serum free medium containing the indicated agents was added, and then the tubes were rephotographed 4 h later (4 h post-peak). For the phase-contrast images acquired at 0 and 4 h, the tubes were traced using the paintbrush function of National Institutes of Health ImageJ. Normalized tube length was calculated by dividing the total pixel units at 4 h (end point) with the total pixel units at 0 h. Data represent the mean ± S.E. of four experiments. Each independent experiment was from quadruplicate wells. *, $p < 0.05$; *ns*, not significant (one-way ANOVA). *B*, representative phase contrast images of HMREC tubes before (0 h, peak) and after (4 h post-peak) addition of the indicated treatments. *Black arrows* point to representative enduring tubes, and *white arrows* denote examples of tubes that regressed. *Scale bar* = 250 μm. *C*, LPA-mediated regression was blocked with LPA receptor antagonists. Tubes were organized as in *A*, and regression was monitored in the presence of the indicated agents. BrP-LPA (20 μM) and Ki16425 (20 μM) are LPA receptor antagonists, whereas HA-130 (10 μM) is an ATX inhibitor (23). *D*, IGF-1 prevented VEGF-A-mediated regression. After generating tubes as described in *A*, VEGF-mediated regression was assayed in the presence of the indicated agents: VEGF-A (2.5 ng/ml), BrP-LPA (20 μM), HA-130 (10 μM), and IGF-1 (100 ng/ml). *E*, insulin failed to oppose LPA-stimulated regression. Tubes were organized as in *A*, and the impact of IGF-1 (100 ng/ml) and insulin (100 ng/ml) to prevent LPA-mediated regression was compared. *, $p < 0.05$; **, $p < 0.01$; ***, $p < 0.001$; ****, $p < 0.0001$.

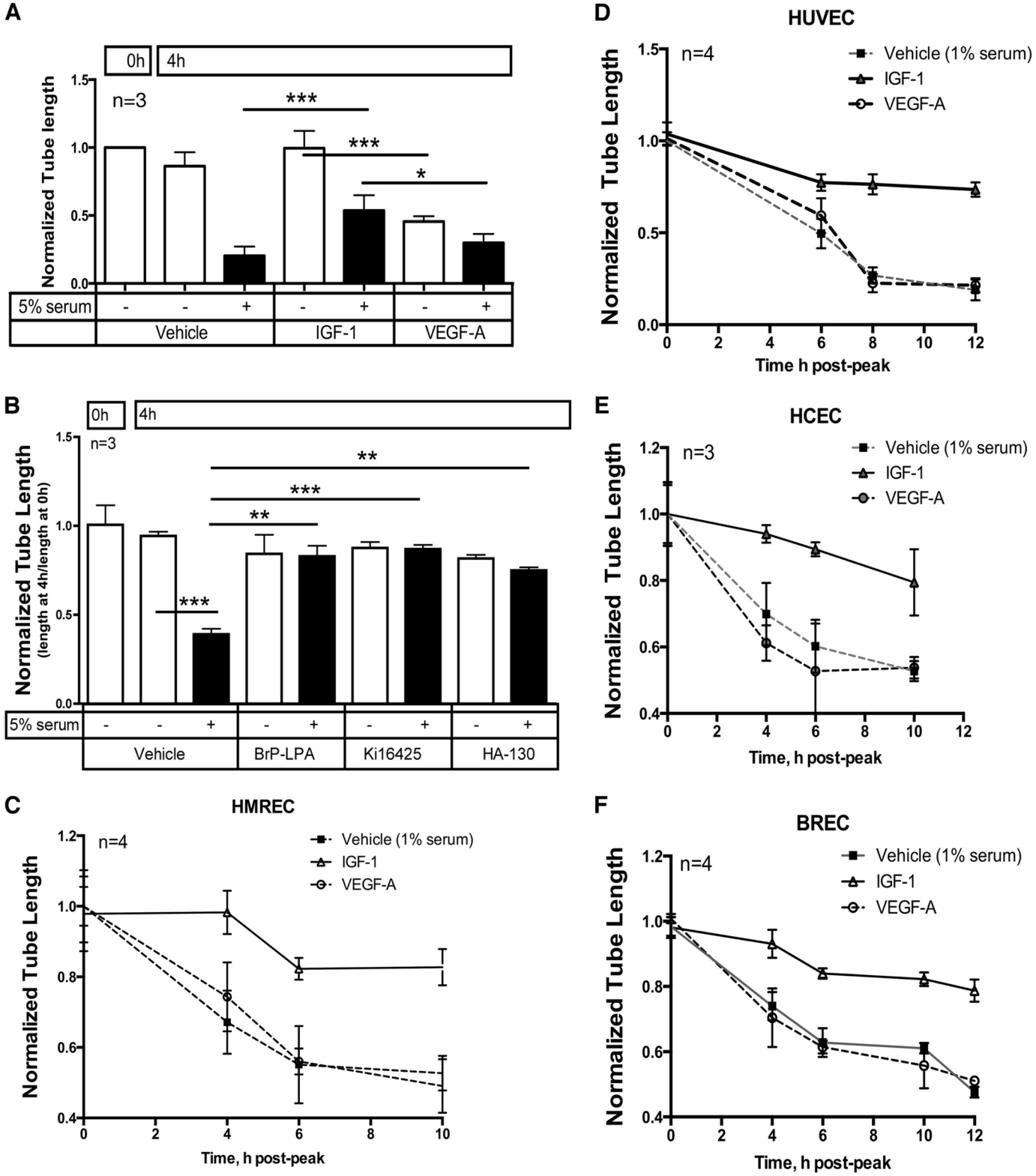

FIGURE 2. **IGF-1 stabilized tubes generated from primary endothelial cells derived from various vascular beds.** *A*, IGF-1 prevented serum-stimulated regression. These experiments were done as in Fig. 1*A*, except that, during the 4-h regression period, the collagen sandwich was overlaid with medium containing 5% (instead of 0%) serum. *B*, serum-stimulated regression was prevented by antagonists of LPA receptors or ATX. These experiments were done as in Fig. 1*C*, except that, during the 4-h regression period, the collagen sandwich was overlaid with medium containing 5% (instead of 0%) serum. *C–F*, IGF-1 antagonized serum-induced regression of tubes organized from four different types of primary endothelial cells. The experiments were done as in *A*, except that, during the regression period, the collagen sandwich was overlaid with medium containing 1% (instead of 5%) serum. Regression of tubes beyond the 4-h time point is also shown. *HUVEC*, human umbilical vein endothelial cell; *BREC*, bovine retinal endothelial cell. *, $p < 0.05$; ***, $p < 0.001$.

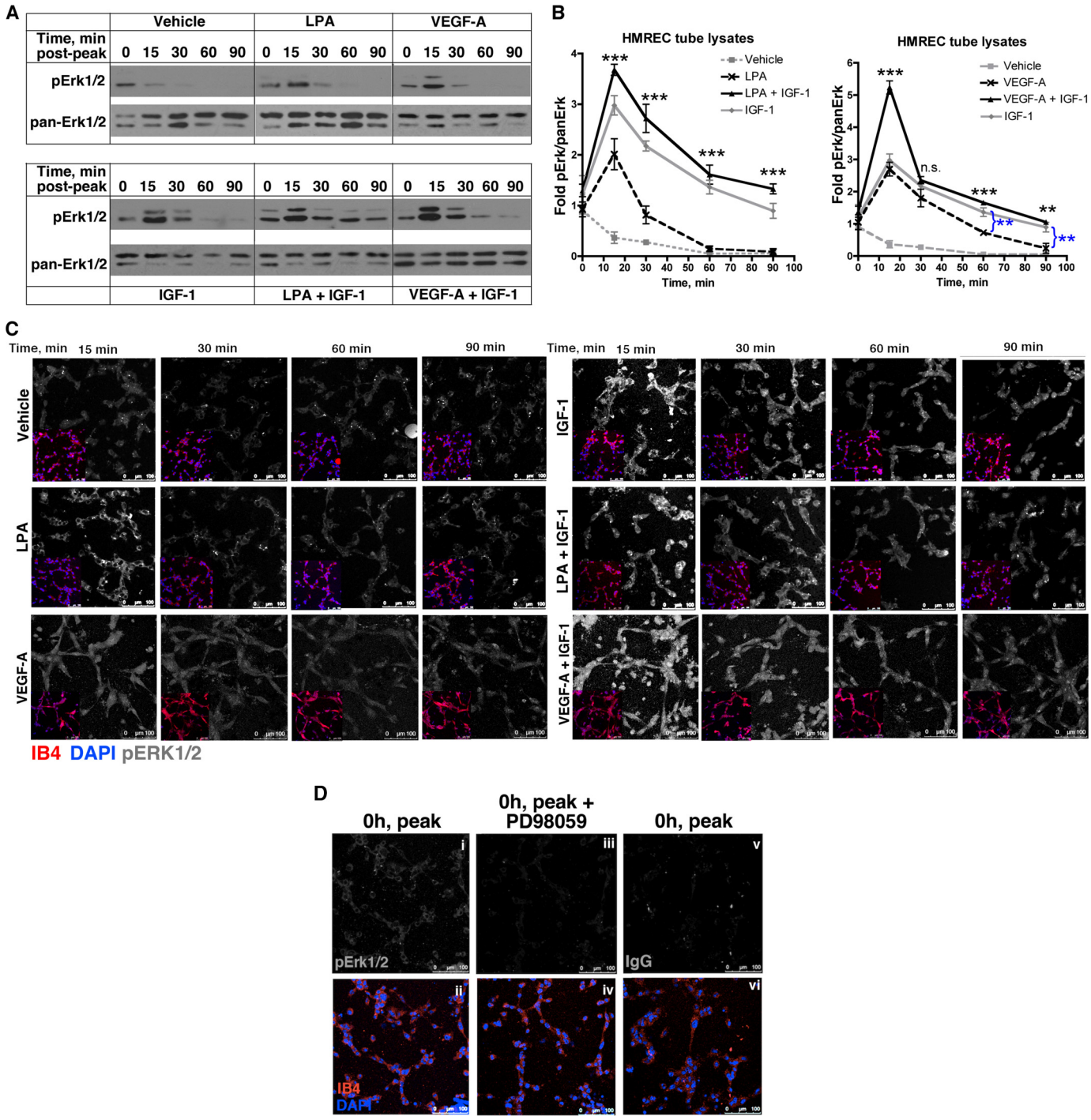

FIGURE 3. **IGF-1-mediated stabilization was associated with enduring activation of Erk.** *A*, HMREC tubes were generated as described in Fig. 1*A*, except that these experiments were performed in 24-well plates. At the indicated time points, tube lysates were extracted and subjected to Western blot analysis. Five wells were pooled for each lane/time point. *B*, the data from three to six independent Western blot experiments were quantified and expressed as a ratio of pErk:panErk. These values were normalized to the average of the unstimulated samples (the 0 time point in *A*), and the mean ± S.E. was plotted. *Asterisks* indicate paired comparisons between LPA or VEGF alone *versus* LPA + IGF-1 or VEGF + IGF-1. **, $p < 0.01$; ***, $p < 0.001$; *ns*, not significant (Student's *t* test). *C*, IGF-1 induced enduring activation of Erk. The *lower left quadrant* shows an inset of the same tubes that were costained with isolectin B4 (which decorates endothelial cells, *red*) and DAPI (nuclei, *blue*). The remainder of each panel is the same magnification as the *lower left quadrant* and shows the staining with an anti-pErk1/2 antibody (shown in *monochrome*). Images are representative of three independent experiments performed in duplicate wells (3 random fields/well). *Scale bar* = 100 μm. *D*, controls to assess the specificity of anti-pErk1/2 immunofluorescent signal. When tubes had formed (0 h, peak, as in Fig. 1*B*), they were stained with the anti-pErk1/2 antibody (*i*) or a non-immune isotype IgG (*vi*). Alternatively, tubes were pretreated with an Erk pathway inhibitor (PD98059, 10 μM) and stained with the anti-pErk1/2 antibody. The *bottom row* (*ii*, *iv*, and *vi*) shows and IB4 and DAPI-stained channels of the *top row*.

substrate lysophosphatidyl choline (30–32). As expected, tubes regressed when 5% serum was present, and this response was suppressed by LPA receptor antagonists (Fig. 2, *A* and *B*). Furthermore, inhibiting ATX prevented serum-driven regression (Fig. 2*B*). These observations indicate a requirement for ATX, which is not only present in serum but also produced by cells

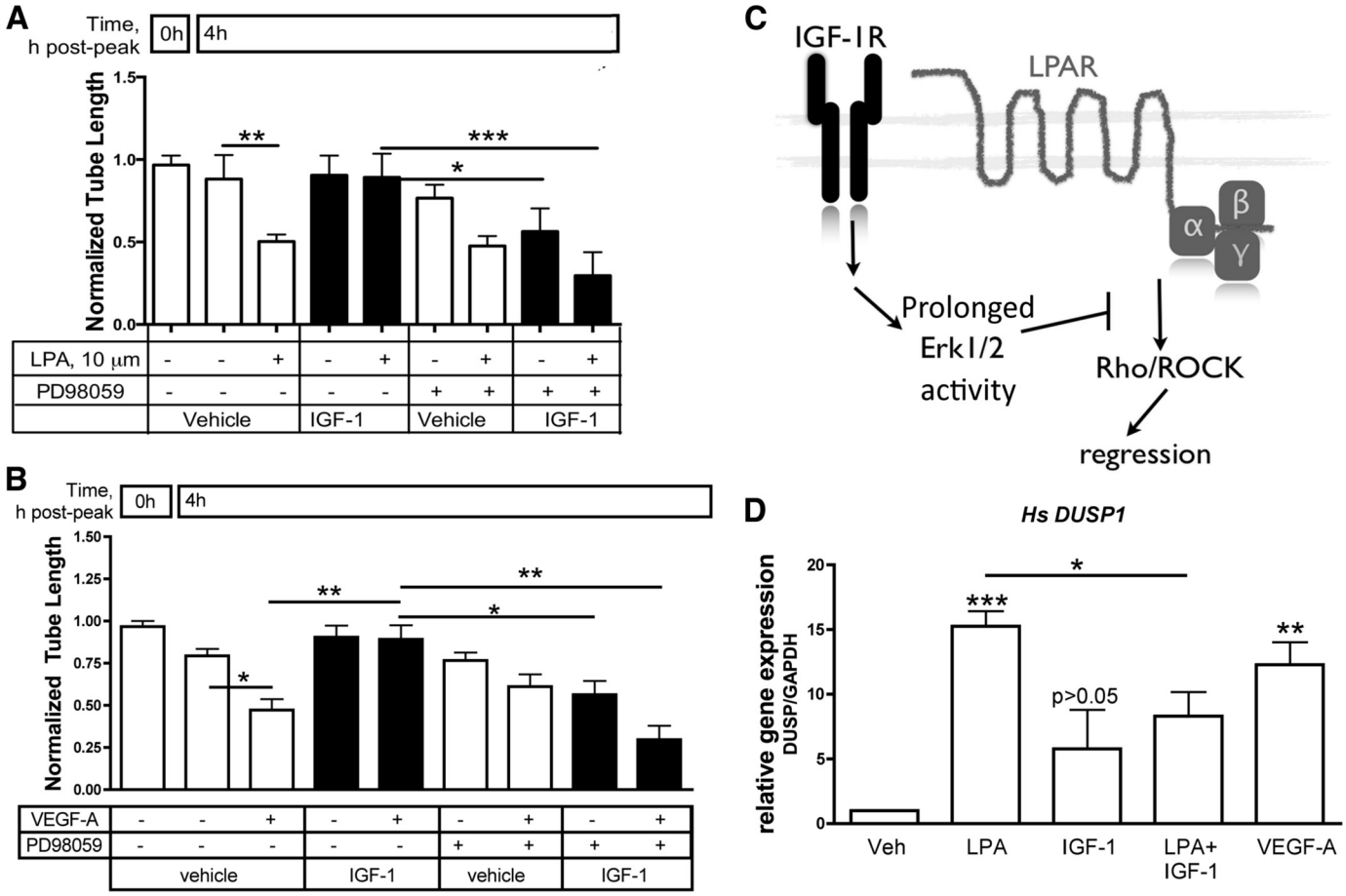

FIGURE 4. **IGF-1-mediated stabilization required Erk activity.** *A* and *B*, tubes were organized as in Fig. 1*A*, and LPA- or VEGF-driven regression was monitored in the presence of the indicated agents. PD98059 is a MEK inhibitor and was used at 10 μM. *, $p < 0.05$; **, $p < 0.01$; ***, $p < 0.001$; $n = 3$; one-way ANOVA. *C*, working model for how IGF-1 prevented regression. IGF-1 triggered prolonged activation of Erk1/2 and, thereby, antagonized Rho/ROCK, which are required for LPA-driven regression (36, 38). *D*, human (*Hs*) *DUSP1*) expression in tubes exposed to LPA, IGF-1, LPA + IGF-1, or VEGF-A. Tubes on a 24-well scale were organized as in Fig. 1*A*, and then LPA (10 μM) alone or in combination with IGF-1 (100 ng/ml) or VEGF (2.5 ng/ml) was added for 30 min. For each treatment, total RNA extracted from five wells was pooled. Target gene expression relative to GAPDH was quantified by the double derivative method after quantitative real-time RT-PCR and expressed as -fold increase relative to vehicle (assigned a value of 1). The data in the *bar graph* are averaged from three independent experiments, and each experiment was performed in duplicate wells. *, $p < 0.05$; **, $p < 0.01$; ***, $p < 0.001$ (one-way ANOVA). *Veh*, vehicle.

(31–34). We observed previously that blocking ATX reduced the level of LPA (35). Importantly, IGF-1 prevented regression under these conditions, whereas VEGF did not and, instead, even augmented regression slightly (Fig. 2*A*), as observed when purified LPA was driving this response (Fig. 1*A*). Even 1% serum was sufficient for regression, and, under these conditions, IGF-1 also stabilized tubes whereas VEGF did not (Fig. 2*C*).

The experiments described so far were performed with primary human retinal microvascular endothelial cells. To test the relevance of these observations to primary endothelial cells derived from additional vascular beds, we repeated the experiment shown in Fig. 2*C* with endothelial cells derived from human umbilical vein, human choroid (HCECs), and bovine retina (bovine microvascular retinal endothelial cells). All three behaved as HMRECs did. They organized into tubes in the presence of VEGF and subsequently regressed when cultured in 1% serum (Fig. 2, *D–F*). IGF-1, but not VEGF, prevented regression (Fig. 2, *D–F*). We conclude that IGF-1 stabilized tubes organized from a variety of endothelial types derived from distinct vascular beds and under various conditions.

The data in Fig. 2, *C* and *D*, also indicate that the rate of regression followed comparable but not identical time courses for all four types of endothelial cells. Possible reasons include differences in expression of LPA receptors and/or responsiveness to LPA or relative expression and basal activation of IGF-1R. The concept that the response to LPA may not be uniform is supported by our recent observation that prolonged exposure of endothelial cells to high glucose blunts their ability to respond to LPA (10, 12, 24), which indicates that LPA responsiveness is not a fixed parameter even within a single cell type.

IGF-1-mediated Stabilization Was Dependent on Erk Activity and Associated with Prolonged Activation—What is the mechanism by which IGF-1 antagonizes LPA-mediated regression? In light of previous publications that IGF-1 activates Erk (29, 30), which antagonizes LPA-stimulated regression (36–38), we considered whether Erk activation was associated with stabilization. In this set of experiments, the regression assay conditions were the same as in Fig. 1 (serum-free medium), and time points that precede overt regression were chosen to compare tubes of similar lengths. Fig. 3, *A* and *B*, shows that LPA, VEGF, and IGF-1 all activated Erk and that, when IGF-1 was present, Erk stayed active longer.

Monitoring Erk activity in tube lysates, as was done in Fig. 3, *A* and *B*, required extraction of the tubes from the collagen gel

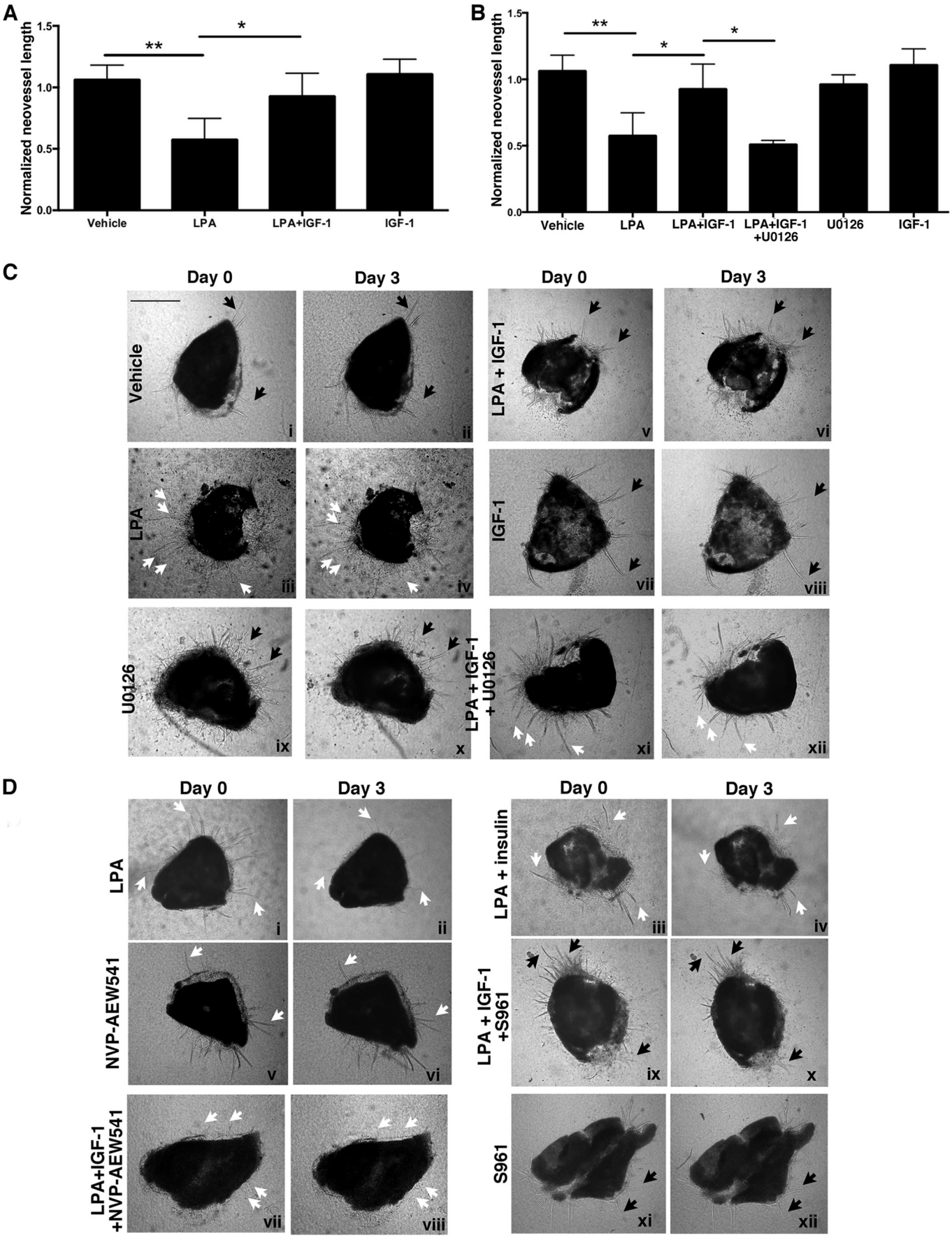
A
Normalized neovessel length
1.5
1.0
0.5
0.0
**
*
Vehicle
LPA
LPA+IGF-1
IGF-1
B
Normalized neovessel length
1.5
1.0
0.5
0.0
**
*
*
Vehicle
LPA
LPA+IGF-1
LPA+IGF-1 +U0126
U0126
IGF-1
C
Day 0
Day 3
Day 0
Day 3
Vehicle
i
ii
LPA + IGF-1
v
vi
LPA
iii
iv
IGF-1
vii
viii
U0126
ix
x
LPA + IGF-1 + U0126
xi
xii
D
Day 0
Day 3
Day 0
Day 3
LPA
i
ii
LPA + insulin
iii
iv
NVP-AEW541
v
vi
LPA + IGF-1 +S961
ix
x
LPA+IGF-1 +NVP-AEW541
vii
viii
S961
xi
xii

(32). Using this approach, we previously reported differences in the phosphorylation state of myosin light chain kinase (10, 12). Although it is difficult to assess to what extent this procedure itself influenced the activation state of Erk, we did observe the predicted differences between stimulated and unstimulated samples.

To further address this caveat, we evaluated Erk activity by immunofluorescence, which did not involve extraction of the tubes from the collagen gel. The same correlation between enduring Erk activity and tube stability was observed using this approach. Erk stayed active longer in tubes exposed to IGF-1 alone or in combination (IGF-1 + VEGF or IGF-1 + LPA) compared with tubes exposed to VEGF or LPA alone (Fig. 3*C*). The pErk1/2 signal is shown in monochrome. Fig. 3*C*, *inset*, shows the Isolectin B4-positive (*IB4*+) endothelial tubes in *red*, and the nuclei are *blue*. The pErk1/2 signal was sensitive to a Mek inhibitor, PD98059, and was not observed when a non-immune isotype control was used (Fig. 3*D*). Therefore, two different approaches indicated that IGF-1-mediated stabilization of tubes was associated with enduring activation of Erk1/2.

In light of the correlation between prolonged Erk activation and stabilization (10, 12, 36, 38), we considered whether Erk was required for IGF-1 to stabilize endothelial tubes. Indeed, two different Erk pathway inhibitors, PD98059 and U0126 (data not shown), prevented IGF-1 from stabilizing tubes. LPA- and VEGF-driven regression proceeded in the face of IGF-1 when Erk activity was blocked (Fig. 4, *A* and *B*, and data not shown). We concluded that IGF-1-mediated stabilization required Erk activity. The results in Figs. 3 and 4 support the conclusion that prolonged Erk activation is required for IGF-1-dependent stabilization. A plausible reason for why short-lived Erk activation is not sufficient to stabilize nascent tubes is that persistent antagonism of LPA-dependent signaling events such as Rho/ROCK is required to prevent regression (Fig. 4*C*) (10, 12, 38–41, 42).

An intriguing question that arises from this set of results is why the dynamics of Erk activity were not the same for distinct agents that are capable of engaging this signaling pathway. Part of the answer may involve distinct mechanisms by which LPA, VEGF, and IGF-1 engage the Erk pathway (43, 44). Furthermore, these agents may not equivalently trigger signaling events that limit the duration of Erk activation, such as the induction of DUSPs, also called MAP kinase phosphatases), which dephosphorylate and thereby inactivate MAP kinase family members, including Erk (45). Indeed, we observed that LPA and VEGF, which activated Erk transiently, induced the expression of *DUSP1* and *DUSP6* (Fig. 4*D* and data not shown). IGF-1, which stimulated prolonged Erk activity, did not increase the expressions of these DUSPs (Fig. 4*D* and data not shown). Furthermore, IGF-1 suppressed the ability of LPA to induce *DUSP1*, *DUSP2*, and *DUSP5* (Fig. 4*D* and data not shown). Therefore, the differential expression of DUSPs was associated with the distinct kinetics of Erk activation by the various agents used in this study.

IGF-1 Stabilized Retinal Neovessels—To extend our *in vitro* findings to a more physiological setting, we determined whether IGF-1 could prevent LPA-mediated regression of neovessels that sprout from mouse retinal explants. In this *ex vivo* setting (10, 12, 22), retinas were isolated from healthy adult mice, minced, and placed between two layers of collagen that were overlaid with serum- and VEGF-A-containing medium. Under these conditions, neovessels are lumenized and consist of IB4+ endothelial cells. They neither grow further nor regress by day 21 (12). Such neovessels decreased in length and appeared less convoluted in response to LPA (Fig. 5, *A* and *C*). We observed that addition of IGF-1 appeared to increase neovessel length in explants that had been otherwise stable over a period of >48 h. However, the enhancement of neovessel outgrowth did not reach statistical significance (Fig. 5, *A* and *C*). Although IGF-1 did not significantly promote growth of the stabilized neovessels, it prevented their regression driven by LPA (Fig. 5, *A* and *C*). Similar to the results with the tube assay, experiments with inhibitors and decoy agonists indicated that IGF-1 was acting primarily through IGF-1R (Fig. 5, *B* and *D*) but not insulin receptor.

To consider the role of the Erk pathway in IGF-1-mediated stabilization of neovessels, we repeated these explant experiments in the presence of an Erk pathway inhibitor, U0126. As shown in Fig. 4, *B* and *C*, inhibiting the Erk pathway had overcome the ability of IGF-1 to stabilize neovessels in the presence of LPA. These results indicate that IGF-1 stabilizes retinal neovessels and that this phenomenon was dependent on the Erk pathway. Furthermore, these *ex vivo* results recapitulate the *in vitro* findings using primary endothelial cells.

DISCUSSION

The data presented here suggest that there is a division of labor among proangiogenic agents. IGF-1 stabilizes nascent vessels whose formation is driven by VEGF. The underlying mechanism of IGF-1-mediated stabilization involves prolonged activation of Erk, which antagonizes LPA-driven regression.

Although our results indicate that Erk activity and, thereby, Rho/ROCK antagonism (36), was required for IGF-1 to stabilize nascent tubes, there may be additional signaling events that

FIGURE 5. **IGF-1 prevented LPA-dependent regression of retinal neovessels, and this phenomenon was dependent on Erk activity.** *A*, IGF-1 antagonized LPA-mediated regression of retinal neovessels. Murine retinal explants were placed in a collagen sandwich and overlaid with serum- and VEGF-containing medium. Neovessels sprouted within 7–10 days and, thereafter, increased in number, length, and caliber through days 18–21. Neovessels that showed no significant outgrowth within a 48-h window were considered stable. Stable neovessels were photographed (*day 0*), endothelial basal medium with 10% serum (vehicle) alone or in combination with the indicated treatments was added, and the neovessels were rephotographed 3 days later (*day 3*). The treatments included LPA (10 μM), IGF-1 (100 ng/ml), the MEK inhibitor U0126 (10 μM), insulin (100 ng/ml), the IGF-1R tyrosine kinase inhibitor NVP-AEW541 (10 μM), and the insulin receptor antagonist S961 (100 nM). Treatments were replenished every 12 h within this 3-day window. For the phase-contrast images acquired at days 0 and 3, the neovessels were traced using the paintbrush function of National Institutes of Health ImageJ. Normalized neovessel length was calculated by dividing the total pixel units at day 3 (end point) with the total pixel units at day 0. Data represent the mean ± S.E. of three mice, and each independent experiment was performed in duplicate (left eye and right eye). *, $p < 0.05$; **, $p < 0.01$ (one-way ANOVA). *B*, blocking the Erk pathway overcame the ability of IGF-1 to prevent LPA-mediated regression of neovessels. Experiments in *A* were repeated in a parallel assay wherein the retinal explants were treated with the MEK inhibitor U0126 at a dose of 10 μM. Data represent the mean ± S.E. of three mice, and each independent experiment was performed in duplicate (left eye and right eye). *, $p < 0.05$; **, $p < 0.01$ (one-way ANOVA). *C* and *D*, representative phase-contrast images of retinal explants at days 0 and 3. *Black arrows* point to representative neovessels that did not regress, and *white arrows* denote examples of neovessels that did regress. *Scale bar* = 250 μm.

play a role during this phase of neovessel remodeling. For instance, in mesenchymal stem cells, IGF-1 induces phosphorylation of p190 RhoGAP and, thereby, results in its translocation and increased ability to inactivate Rho (46). This suggests that, in addition to activating Erk, IGF-1R signaling may induce Rho inactivation via alternate routes. It would be interesting to see whether this particular alternate route to Rho inactivation also operates in vascular endothelial cells.

To begin to understand why IGF-1 activated Erk longer than either VEGF or LPA, we focused on DUSPs. Our results indicate that VEGF and LPA stimulated an increase in *DUSP1*, whereas as IGF-1 did not (Fig. 4*D*). Consequently, the faster decline in Erk activity in tubes exposed to LPA or VEGF alone may be, at least in part, due to an inducible increase in the expression of certain DUSPs. We also observed that IGF-1 promoted translocation of activated Erk to the nucleus (Fig. 3*C*) (47, 48). It would be interesting to know whether nuclear translocation protects Erk from dephosphorylation and/or results in transcriptional modifications that contribute to the persistence of nascent capillaries.

Given that Erk contributes to the migration of cells, it was somewhat of a surprise that antagonizing the Erk pathway suppressed LPA-dependent regression, which involves cell migration. A likely explanation emerges when one considers cell types in which the Erk pathway is required for migration. In vascular smooth muscle cells, blocking the Erk pathway reduces PDGF-driven migration, whereas this intervention has no effect on fibroblasts (49–51). Similarly, LPA or VEGF-stimulated migration of endothelial cells is unaffected by Erk pathway antagonists (52, 53). In this context (Fig. 4*C* and Refs. 10, 12, 36), Erk antagonized LPA-driven regression because it suppressed Rho/ROCK, which was essential for this response.

Acknowledgments—We thank Mary Elizabeth Hartnett (University of Utah) for HCECs and David Anotnetti and Xuwen Lin (Kellogg Eye Center, University of Michigan) for advice on how to prepare lysates of endothelial cell tubes. We also thank Maximilian Gerhardt for technical assistance with some of the experiments.

REFERENCES

1. Carmeliet, P., and Jain, R. K. (2011) Molecular mechanisms and clinical applications of angiogenesis. *Nature* **473,** 298–307
2. Augustin, H. G., Koh, G. Y., Thurston, G., and Alitalo, K. (2009) Control of vascular morphogenesis and homeostasis through the angiopoietin-Tie system. *Nat. Rev. Mol. Cell Biol.* **10,** 165–177
3. Im, E., and Kazlauskas, A. (2006) New insights regarding vessel regression. *Cell Cycle* **5,** 2057–2059
4. Ferrara, N., and Kerbel, R. S. (2005) Angiogenesis as a therapeutic target. *Nature* **438,** 967–974
5. Darland, D. C., and D'Amore, P. A. (1999) Blood vessel maturation: vascular development comes of age. *J. Clin. Invest.* **103,** 157–158
6. Goede, V., Schmidt, T., Kimmina, S., Kozian, D., and Augustin, H. G. (1998) Analysis of blood vessel maturation processes during cyclic ovarian angiogenesis. *Lab. Invest.* **78,** 1385–1394
7. Hanahan, D. (1997) Signaling vascular morphogenesis and maintenance. *Science* **277,** 48–50
8. Holash, J., Maisonpierre, P. C., Compton, D., Boland, P., Alexander, C. R., Zagzag, D., Yancopoulos, G. D., and Wiegand, S. J. (1999) Vessel cooption, regression, and growth in tumors mediated by angiopoietins and VEGF. *Science* **284,** 1994–1998
9. Rao, S., Lobov, I. B., Vallance, J. E., Tsujikawa, K., Shiojima, I., Akunuru, S., Walsh, K., Benjamin, L. E., and Lang, R. A. (2007) Obligatory participation of macrophages in an angiopoietin 2-mediated cell death switch. *Development* **134,** 4449–4458
10. Im, E., Motiejunaite, R., Aranda, J., Park, E. Y., Federico, L., Kim, T. I., Clair, T., Stracke, M. L., Smyth, S., and Kazlauskas, A. (2010) Phospholipase Cγ activation drives increased production of autotaxin in endothelial cells and lysophosphatidic acid-dependent regression. *Mol. Cell Biol.* **30,** 2401–2410
11. Aranda, J., Motiejunaite, R., Im, E., and Kazlauskas, A. (2012) Diabetes disrupts the response of retinal endothelial cells to the angiomodulator lysophosphatidic Acid. *Diabetes* **61,** 1225–1233
12. Aranda, J., Motiejunaite, R., Silva, P., Aiello, L. P., and Kazlauskas, A. (2013) Regression activity that is naturally present in vitreous becomes ineffective as patients develop proliferative diabetic retinopathy. *Diabetologia* **56,** 1444–1453.
13. Hellström, A., Engström, E., Hård, A. L., Albertsson-Wikland, K., Carlsson, B., Niklasson, A., Löfqvist, C., Svensson, E., Holm, S., Ewald, U., Holmström, G., and Smith, L. E. (2003) Postnatal serum insulin-like growth factor I deficiency is associated with retinopathy of prematurity and other complications of premature birth. *Pediatrics* **112,** 1016–1020
14. Löfqvist, C., Andersson, E., Sigurdsson, J., Engström, E., Hård, A. L., Niklasson, A., Smith, L. E., and Hellström, A. (2006) Longitudinal postnatal weight and insulin-like growth factor I measurements in the prediction of retinopathy of prematurity. *Arch. Ophthalmol.* **124,** 1711–1718
15. Löfqvist, C., Engström, E., Sigurdsson, J., Hård, A. L., Niklasson, A., Ewald, U., Holmström, G., Smith, L. E., and Hellström, A. (2006) Postnatal head growth deficit among premature infants parallels retinopathy of prematurity and insulin-like growth factor-1 deficit. *Pediatrics* **117,** 1930–1938
16. Hellström, A., Carlsson, B., Niklasson, A., Segnestam, K., Boguszewski, M., de Lacerda, L., Savage, M., Svensson, E., Smith, L., Weinberger, D., Albertsson Wikland, K., and Laron, Z. (2002) IGF-I is critical for normal vascularization of the human retina. *J. Clin. Endocrinol. Metab.* **87,** 3413–3416
17. Smith, L. E., Shen, W., Perruzzi, C., Soker, S., Kinose, F., Xu, X., Robinson, G., Driver, S., Bischoff, J., Zhang, B., Schaeffer, J. M., and Senger, D. R. (1999) Regulation of vascular endothelial growth factor-dependent retinal neovascularization by insulin-like growth factor-1 receptor. *Nat. Med.* **5,** 1390–1395
18. Kondo, T., Vicent, D., Suzuma, K., Yanagisawa, M., King, G. L., Holzenberger, M., and Kahn, C. R. (2003) Knockout of insulin and IGF-1 receptors on vascular endothelial cells protects against retinal neovascularization. *J. Clin. Invest.* **111,** 1835–1842
19. Ruan, G. X., and Kazlauskas, A. (2012) Axl is essential for VEGF-A-dependent activation of PI3K/Akt. *EMBO J.* **31,** 1692–1703
20. Jacobo, S. M., Deangelis, M. M., Kim, I. K., and Kazlauskas, A. (2013) Age-related macular degeneration-associated silent polymorphisms in HtrA1 impair its ability to antagonize insulin-like growth factor 1. *Mol. Cell Biol.* **33,** 1976–1990
21. Antonetti, D. A., Klein, R., and Gardner, T. W. (2012) Diabetic retinopathy. *N. Engl. J. Med.* **366,** 1227–1239
22. Im, E., Venkatakrishnan, A., and Kazlauskas, A. (2005) Cathepsin B regulates the intrinsic angiogenic threshold of endothelial cells. *Mol. Biol. Cell* **16,** 3488–3500
23. Albers, H. M., Dong, A., van Meeteren, L. A., Egan, D. A., Sunkara, M., van Tilburg, E. W., Schuurman, K., van Tellingen, O., Morris, A. J., Smyth, S. S., Moolenaar, W. H., and Ovaa, H. (2010) Boronic acid-based inhibitor of autotaxin reveals rapid turnover of LPA in the circulation. *Proc. Natl. Acad. Sci. U.S.A.* **107,** 7257–7262
24. Park, E. Y., and Kazlauskas, A. (2012) Primary human endothelial cells secrete agents that reduce responsiveness to lysophosphatidic acid (LPA). *Biosci. Rep.* **32,** 393–400
25. Benjamin, L. E., Hemo, I., and Keshet, E. (1998) A plasticity window for blood vessel remodelling is defined by pericyte coverage of the preformed endothelial network and is regulated by PDGF-B and VEGF. *Development* **125,** 1591–1598
26. Benjamin, L. E., Golijanin, D., Itin, A., Pode, D., and Keshet, E. (1999) Selective ablation of immature blood vessels in established human tumors

follows vascular endothelial growth factor withdrawal. *J. Clin. Invest.* **103,** 159–165
27. Ptaszynska, M. M., Pendrak, M. L., Stracke, M. L., and Roberts, D. D. (2010) Autotaxin signaling via lysophosphatidic acid receptors contributes to vascular endothelial growth factor-induced endothelial cell migration. *Mol. Cancer Res.* **8,** 309–321
28. Tanaka, M., Okudaira, S., Kishi, Y., Ohkawa, R., Iseki, S., Ota, M., Noji, S., Yatomi, Y., Aoki, J., and Arai, H. (2006) Autotaxin stabilizes blood vessels and is required for embryonic vasculature by producing lysophosphatidic acid. *J. Biol. Chem.* **281,** 25822–25830
29. Kayali, A. G., Eichhorn, J., Haruta, T., Morris, A. J., Nelson, J. G., Vollenweider, P., Olefsky, J. M., and Webster, N. J. (1998) Association of the insulin receptor with phospholipase C-γ (PLCγ) in 3T3-L1 adipocytes suggests a role for PLCγ in metabolic signaling by insulin. *J. Biol. Chem.* **273,** 13808–13818
30. Seely, B. L., Reichart, D. R., Staubs, P. A., Jhun, B. H., Hsu, D., Maegawa, H., Milarski, K. L., Saltiel, A. R., and Olefsky, J. M. (1995) Localization of the insulin-like growth factor I receptor binding sites for the SH2 domain proteins p85, Syp, and GTPase activating protein. *J. Biol. Chem.* **270,** 19151–19157
31. Yung, Y. C., Stoddard, N. C., and Chun, J. (2014) LPA receptor signaling: pharmacology, physiology, and pathophysiology. *J. Lipid Res.* **55,** 1192–1214
32. Cheng, H. Y., Dong, A., Panchatcharam, M., Mueller, P., Yang, F., Li, Z., Mills, G., Chun, J., Morris, A. J., and Smyth, S. S. (2012) Lysophosphatidic acid signaling protects pulmonary vasculature from hypoxia-induced remodeling. *Arterioscler. Thromb. Vasc. Biol.* **32,** 24–32
33. Teo, S. T., Yung, Y. C., Herr, D. R., and Chun, J. (2009) Lysophosphatidic acid in vascular development and disease. *IUBMB Life* **61,** 791–799
34. Stortelers, C., Kerkhoven, R., and Moolenaar, W. H. (2008) Multiple actions of lysophosphatidic acid on fibroblasts revealed by transcriptional profiling. *BMC Genomics* **9,** 387
35. Motiejūnaitė, R., Aranda, J., and Kazlauskas, A. (2014) Pericytes prevent regression of endothelial cell tubes by accelerating metabolism of lysophosphatidic acid. *Microvasc. Res.* **93,** 62–71
36. Mavria, G., Vercoulen, Y., Yeo, M., Paterson, H., Karasarides, M., Marais, R., Bird, D., and Marshall, C. J. (2006) ERK-MAPK signaling opposes Rho-kinase to promote endothelial cell survival and sprouting during angiogenesis. *Cancer Cell* **9,** 33–44
37. Im, E., and Kazlauskas, A. (2006) Regulating angiogenesis at the level of PtdIns-4,5-P2. *EMBO J.* **25,** 2075–2082
38. Im, E., and Kazlauskas, A. (2007) Src family kinases promote vessel stability by antagonizing the Rho/ROCK pathway. *J. Biol. Chem.* **282,** 29122–29129
39. Hoang, M. V., Nagy, J. A., and Senger, D. R. (2011) Active Rac1 improves pathologic VEGF neovessel architecture and reduces vascular leak: mechanistic similarities with angiopoietin-1. *Blood* **117,** 1751–1760
40. Hoang, M. V., Whelan, M. C., and Senger, D. R. (2004) Rho activity critically and selectively regulates endothelial cell organization during angiogenesis. *Proc. Natl. Acad. Sci. U.S.A.* **101,** 1874–1879
41. Connolly, J. O., Simpson, N., Hewlett, L., and Hall, A. (2002) Rac regulates endothelial morphogenesis and capillary assembly. *Mol. Biol. Cell* **13,** 2474–2485
42. Roberts, D. D. (2011) Activate Rac to rescue new vessels. *Blood* **117,** 1444–1445
43. Grammer, T. C., and Blenis, J. (1997) Evidence for MEK-independent pathways regulating the prolonged activation of the ERK-MAP kinases. *Oncogene* **14,** 1635–1642
44. Lin, S. C., Chien, C. W., Lee, J. C., Yeh, Y. C., Hsu, K. F., Lai, Y. Y., Lin, S. C., and Tsai, S. J. (2011) Suppression of dual-specificity phosphatase-2 by hypoxia increases chemoresistance and malignancy in human cancer cells. *J. Clin. Invest.* **121,** 1905–1916
45. Caunt C. J., and Keyse S. M. (2013) Dual-specificity MAP kinase phosphatases (MKPs): shaping the outcome of MAP kinase signaling. *FEBS J.* **280,** 489–504
46. Sordella, R., Jiang, W., Chen, G. C., Curto, M., and Settleman, J. (2003) Modulation of Rho GTPase signaling regulates a switch between adipogenesis and myogenesis. *Cell* **113,** 147–158
47. Kwon, H., Jeong, K., Hwang, E. M., Park, J. Y., and Pak, Y. (2011) A novel domain of caveolin-2 that controls nuclear targeting: regulation of insulin-specific ERK activation and nuclear translocation by caveolin-2. *J. Cell Mol. Med.* **15,** 888–908
48. Chen, R. H., Sarnecki, C., and Blenis, J. (1992) Nuclear localization and regulation of erk- and rsk-encoded protein kinases. *Mol. Cell Biol.* **12,** 915–927
49. Pukac, L., Huangpu, J., Karnovsky, M. J. (1998) Platelet-derived growth factor-BB, insulin-like growth factor-I, and phorbol ester activate different signaling pathways for stimulation of vascular smooth muscle cell migration. *Exp. Cell Res.* **242,** 548–560
50. Graf, K., Xi, X. P., Yang, D., Fleck, E., Hsueh, W. A., and Law, R. E. (1997). Mitogen-activated protein kinase activation is involved in platelet-derived growth factor-directed migration by vascular smooth muscle cells. *Hypertension* **29,** 334–339
51. Anand-Apte, B., Zetter, B. R., Viswanathan, A., Qiu, R. G., Chen, J., Ruggieri, R., and Symons, M. (1997) Platelet-derived growth factor and fibronectin-stimulated migration are differentially regulated by the Rac and extracellular signal-regulated kinase pathways. *J. Biol. Chem.* **272,** 30688–30692
52. Panetti, T. S., Nowlen, J., and Mosher, D. F. (2000) Sphingosine-1-phosphate and lysophosphatidic acid stimulate endothelial cell migration. *Arterioscler. Thromb. Vasc. Biol.* **20,** 1013–1019
53. Meadows, K. N., Bryant, P., and Pumiglia, K. (2001) Vascular endothelial growth factor induction of the angiogenic phenotype requires Ras activation. *J. Biol. Chem.* **276,** 49289–49298